

Design of Hierarchical Three-Dimensional Printed Scaffolds Considering Mechanical and Biological Factors for Bone Tissue Engineering

Paul F. Egan¹

Department of Health Sciences and Technology,
ETH Zurich,
Honggerberggring 64,
Zurich 8093, Switzerland
e-mail: pegan@ethz.ch

Stephen J. Ferguson

Department of Health Sciences and Technology,
Institute for Biomechanics,
ETH Zurich,
Honggerberggring 64,
Zurich 8093, Switzerland
e-mail: sferguson@ethz.ch

Kristina Shea

Department of Mechanical and Process
Engineering,
ETH Zurich,
Zurich 8092, Switzerland
e-mail: kshea@ethz.ch

Computational approaches have great potential for aiding clinical product development by finding promising candidate designs prior to expensive testing and clinical trials. Here, an approach for designing multilevel bone tissue scaffolds that provide structural support during tissue regeneration is developed by considering mechanical and biological perspectives. Three key scaffold design properties are considered: (1) porosity, which influences potential tissue growth volume and nutrient transport, (2) surface area, which influences biodegradable scaffold dissolution rate and initial cell attachment, and (3) elastic modulus, which influences scaffold deformation under load and, therefore, tissue stimulation. Four scaffold topology types are generated by patterning beam or truss-based unit cells continuously or hierarchically and tuning the element diameter, unit cell length, and number of unit cells. Parametric comparisons suggest that structures with truss-based scaffolds have higher surface areas but lower elastic moduli for a given porosity in comparison to beam-based scaffolds. Hierarchical scaffolds possess a large central pore that increases porosity but lowers elastic moduli and surface area. Scaffold samples of all topology types are 3D printed with dimensions suitable for scientific testing. A hierarchical scaffold is fabricated with dimensions and properties relevant for a spinal interbody fusion cage with a maximized surface-volume ratio, which illustrates a potentially high performing design configured for mechanical and biological factors. These findings demonstrate the merit in using multidisciplinary and computational approaches as a foundation of tissue scaffold development for regenerative medicine. [DOI: 10.1115/1.4036396]

1 Introduction

Engineering design has great potential for aiding clinical product development, especially for systems operating on mechanical and biological principles [1–3]. Products frequently underperform in clinical trials and fail to reach the market, which results in financial losses [4–7]. Computational approaches for developing tissue scaffolds are particularly useful due to emerging 3D printing processes and design methods [8–11]. Tissue scaffolds are porous structures that mechanically bear load while facilitating biological tissue growth. Scaffold optimization is challenging due to complex couplings in mechanical loads and biological behavior [12]. Scaffold design typically relies on trial-and-error [13], which suggests an opportunity for developing improved engineering design approaches. Computational design approaches may reduce research and development costs for preclinical trial product development while improving scaffold performance [14–17]. Here, we address a subset of design challenges for 3D printed tissue scaffolds inspired by bone's hierarchical structure.

Mechanical design is relevant to bone tissue engineering, since mechanical stimulation and scaffold geometry influence bone growth and strength [18–21]. Spinal interbody fusion cage systems utilize scaffolds to facilitate vertebral fusion after surgical intervertebral disc removal [22–26]. The treatment's goal is to generate new rigid bone tissue that fuses two adjacent vertebrae

into one continuous bone structure. An interbody fusion cage is inserted to provide temporary structural support and a biological niche for bone fusion.

In interbody fusion cage systems, a porous scaffold is often surrounded by a solid shell structure in direct contact with vertebrae. The solid shell aids in load bearing in addition to hardware, such as pedicle screws that are inserted in adjacent vertebrae. Design approaches with modular units [27,28] are desirable since they facilitate economical testing of scaffold samples that may be patterned within an interbody fusion cage (Fig. 1). While interbody fusion cage products encompass all components required for clinical bone fusion, including supporting hardware and the cage itself, in this work, we focus on the porous scaffold design within the cage.

Figure 1 illustrates an experiment with a mechanical loading device that cyclically applies force to a scaffold sample in cell culture for tissue growth measurements [29,30]. The cycling and

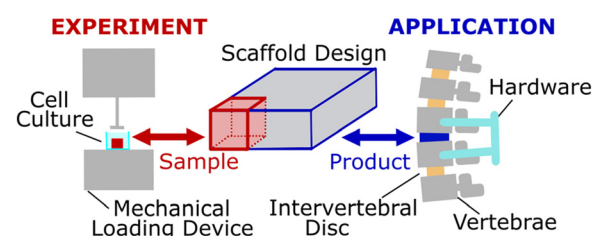


Fig. 1 Design approach for testing scaffold samples rescaled for interbody fusion cage products

¹Corresponding author.

Contributed by the Design Automation Committee of ASME for publication in the JOURNAL OF MECHANICAL DESIGN. Manuscript received December 3, 2016; final manuscript received March 18, 2017; published online April 24, 2017. Assoc. Editor: Katja Holttä-Otto.

loading magnitude are adjustable to emulate spinal loading. Since hardware beyond the scaffold is tunable for altering how load is experienced, we approach the design by initially concentrating on scaffold form properties for tissue growth, rather than its load bearing capabilities. Porosity, pore size, and surface area are key properties that influence tissue growth, in addition to the stiffness and scaffold material biocompatibility. There is a broad range of biocompatible materials [31,32] suitable for tissue scaffolds that could provide acceptable load bearing capabilities once other system components are configured.

This paper aims to demonstrate the merits of using mechanical and biological perspectives for tissue scaffold design, through considering 3D printing fabrication processes, structural design, scaffold properties, and eventual performance [33]. A computational design approach is developed for configuring a scaffold's structure and evaluating its properties. Scaffolds are configured for experiments or for interbody cages and fabricated using stereolithography 3D printing [10]. The paper contributes to mechanical design by introducing the foundations of a design approach to improve upon "trial-and-error" approaches commonly used for tissue scaffolds.

2 Background

Tissue engineering is a multidisciplinary research field that requires mechanical and biological considerations. Literature is reviewed for design and manufacturing of bone tissue scaffolds.

2.1 Scaffold Structure. Scaffold performance is directly related to its structural design, with porosity and pore size being common properties linked to performance [34]. Porosity is the ratio between the void scaffold volume to total nominal volume. Pore size refers to the size of cavities throughout a scaffold. Optimized scaffold designs generally aim for maximizing porosity without compromising mechanical integrity due to lowering material volume. Porosities of 50–85% are typically used for bone tissue scaffolds [35]. Pore sizes are typically between 200 μm and 1000 μm [18]; smaller pores within this range tend to facilitate faster tissue growth while larger pores provide space for unrestricted nutrient transport.

Determining optimal scaffold properties is challenging due to complex couplings of mechanical loads on biological behavior. Evaluation typically requires expensive simulations or wet-lab experiments [12]. Scaffold stiffness at a given porosity can vary considerably depending on its topological organization. Finite element methods show that 3D printed scaffolds with elements at right angles can have high compressive or high shear strength, but more complex geometries are required for high performance in compression and shear [36]. Compression is the primary loading of spinal scaffolds [24], although shear and torsion are also experienced. Forces experienced by the scaffold affect tissue growth rate and type [12]. These complexities suggest the need to concentrate on a scaffold's form prior to fine tuning its mechanics with the interbody cage system as a whole.

2.2 Scaffold Manufacturing. There are numerous fabrication processes suitable for constructing scaffolds with pore sizes and materials relevant to bone tissue engineering. Stochastic foam structures with a distribution of pore sizes are commonly used [18,37]. The distribution of pore sizes mimics bone's natural hierarchy, with small pores to facilitate high surface area and initial cell attachment and larger pores for nutrient transport and vascularization [37]. Stochastic foams are limited mechanically because there is no precise control over material placement, which is enabled by 3D printing [38]. Stereolithography is particularly suitable for 3D printing complex geometries with pores of a few hundred microns [10,39,40].

Biocompatibility is a key material requirement and includes nontoxicity to surrounding tissues [41,42]. Suitable scaffold

materials include specific biocompatible forms of ceramics, polymers, composites, and metals [18,31,32]. It is also desirable for scaffolds to disintegrate in the body, but scaffolds that degrade too fast could lead to mechanical failure if there is not enough new tissue growth to support mechanical loads [32,43,44]. Titanium scaffolds that do not degrade are common but have a high elastic modulus in comparison to bone that may cause stress shielding [36] resulting in weaker bone growth.

2.3 Scaffold Design. Parametric design is often conducted to explore trade-offs in scaffold structural design, properties, and performance [13,45]. One of the earliest computational design approaches generated scaffolds by patterning unit cells with beam elements [46,47] that resulted in the computer-aided system for tissue scaffolds (CASTS) system for generating unit cell libraries [17]. The approach assessed scaffold structural properties including porosity, pore size, and surface area. Performance evaluation is possible through simulations, such as mechanoregulation algorithms for spinal fusion [24]. Simulations are typically expensive, so topologies are generally not redesigned during simulation design exploration, although parametric features such as pore size are tuned [13]. We, therefore, use an approach for initially configuring scaffolds of different topologies and then fine-tuning them parametrically in relation to property assessments.

Bone tissue engineering approaches commonly use bioinspiration to propose structures that recreate the mechanical environment of bone [37], which is well aligned with recent developments in bio-based [1–3] and bio-inspired [48–51] mechanical design. Interbody cage design may benefit from mimicking the natural hierarchy of bone with small and large pores for supporting tissue growth. Further design considerations beyond mimicry are required, since interbody cages aim to generate bone tissue to fuse vertebrae where bone does not exist naturally.

3 Design Approach

A multilevel parametric design approach is used to generate scaffolds with properties linked to mechanical and biological scaffold performance.

3.1 Scaffold Properties. Comparing scaffold properties is efficient for isolating potentially high-performing scaffolds prior to expensive simulation or wet-lab assessments. Porosity, surface area, and elastic modulus properties and their links to mechanical and biological factors relevant to scaffold performance [29] are highlighted in Table 1.

Higher porosity provides more void volume for tissue growth and is typically maximized while not compromising the scaffold's mechanical integrity. Scaffolds need high porosity to promote vasculature growth and facilitate nutrient transport, such as oxygen. Scaffolds that achieve high porosity via many small pores ($\sim 200 \mu\text{m}$ or less) will have a high surface area that promotes initial cell attachment to the scaffold, while scaffolds with larger pores ($\sim 800 \mu\text{m}$ or greater) have better nutrient transport since they are generally more conducive to fluid flow and vasculature growth. A biodegradable scaffold with a high surface area may compromise the mechanical integrity of the structure if the material degrades faster than load bearing tissue is generated [43,44].

Scaffolds with lattice structures may be considered aggregate materials with intrinsic material properties independent of their base material. The ratio between the scaffold's elastic modulus and base material's elastic modulus should generally remain the same regardless of material used. Elastic modulus is inversely proportional to porosity for a given lattice topology, since it is proportional to relative density. Scaffolds of similar porosity could have highly varying elastic moduli based on their topology.

It is essential to compare scaffolds with contrasting topologies by controlling properties such as porosity to isolate how scaffold topology influences performance. Although porosity and elastic

Table 1 Scaffold properties linked to mechanical and biological factors

Scaffold	Mechanical factors	Biological factors
Porosity	Increasing porosity increases void volume for tissue growth	Increasing porosity improves nutrient transport for biological activity
Surface area	Increasing surface area leads to faster disintegration of biodegradable scaffolds	Increasing surface area provides more locations for initial cell attachment
Elastic modulus	Increasing elastic modulus reduces loaded scaffold deformation	Modulates mechanical tissue stimulation that influences tissue growth rate and type

modulus scale with scaffold volume, surface area must be divided by volume to reach a scalable surface–volume ratio [8]. Comparing scaffolds with scalable properties enables economic testing of scaffold samples that retain their properties when rescaled for specific applications.

3.2 Multilevel Design. A multilevel organization is used to design scaffolds since it enables hierarchical topology generation strategies with small and large pores that mimic bone's hierarchy [37]. Hierarchical scaffolds are manufacturable through emerging 3D printing approaches that construct porous structures with microscale resolution [39,40]. Scaffolds designed using beam elements that perform well in compression-dominated loading [52] could outperform commonly used foams that do not have tailored material placement. Multilevel scaffolds are organized across four levels, with lower levels made up of repeatable units used to construct higher levels (Fig. 2).

The lowest level is a beam element with decisions concerning cross-sectional shape (octagonal in Fig. 2) and material. Beam elements form a first-order unit cell structure at Level 1, with decisions concerning how many elements make up a unit cell and their connectivity (cubic in Fig. 2). A second-order unit cell at Level 2 consists of first-order unit cells to create a larger unit cell (hierarchical generated via recursion in Fig. 2, such that the second-order unit cell has the same cubic connectivity as the first-order unit cell). The level 3 tailored structure patterns second-order unit cells to form a rectangular shape for placement in localized areas of the body, such as the spine.

The multilevel design scheme promotes decisions across scales and appropriate use of organizational features at relevant scales. For instance, a recursive hierarchical strategy is beneficial when forming second-order unit cells from first-order unit cells, because it creates unit cells of small and large pores that may promote cell attachment and nutrient transport, respectively. Another recursive hierarchical level from level 2 to level 3 is not necessarily beneficial for bone tissue engineering and instead the modular second unit cells are patterned to form a tailored structure with dimensions suitable for an interbody cage.

Optimization requires decisions that influence parameter relationships within and across levels. Changing beam length alters first-order unit cell size, and therefore, the number of first-order unit cells required to generate a scaffold with appropriate dimensions. Since each first-order unit cell represents a single pore, changing an element's length may influence both tissue growth

and scaffold stiffness. Such interlevel coupling can lead to nonobvious relationships and difficult to traverse design spaces [3], thus further motivating the need for appropriate design methods to aid decision making.

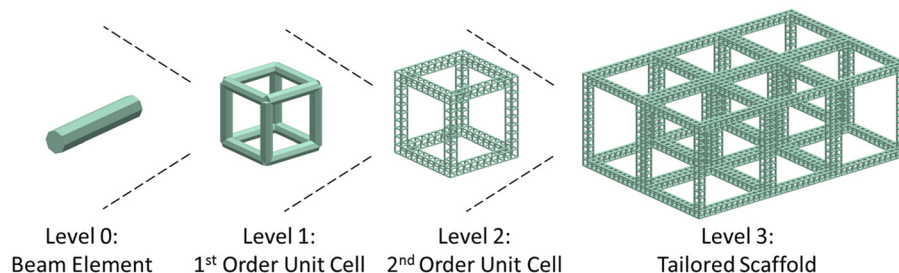
3.3 Topology Types. Second-order unit cells are used for comparing property trade-offs, since second-order unit cells are the highest level generated via hierarchical recursion and are patterned to form a tailored structure that should retain similar properties to individual second-order unit cells. Four second-order unit cells are generated by patterning first-order unit cells continuously or hierarchically and varying the first-order unit cell connectivity. Two first-order connectivities are considered: a beam-based unit cell of twelve elements with six faces and a truss-based unit cell that adds a diagonal element on each face. Although both unit cell types consist of beam elements, the nomenclature refers to the suitability for modeling truss-based cell elements as pin jointed members due to their connectivity.

Continuous second-order unit cell structures consist of regularly patterned first-order unit cells, while hierarchy is achieved by patterning first-order unit cells to form a second-order unit cell with the same connectivity as the first-order unit cell. Topology types formed by each pair-wise combination of first- and second-order unit cell organizations are referred to as continuous beam, hierarchical beam, continuous truss, and hierarchical truss topology types as illustrated in Fig. 3.

Beam-based scaffolds should have higher compressive stiffness when compared to truss-based scaffolds [36], but truss-based scaffolds could favorably increase surface–volume ratios and better resist complex, multi-axial loading. The primary difference between continuous and hierarchical scaffold samples is the large central pore that emerges in hierarchical patterning, which is potentially advantageous since nutrient transport is typically poor in a scaffold's center [53]. Trade-offs concerning porosity, surface–volume ratio, and elastic modulus are possible to explore by tuning parameters describing each topology type's structural design.

3.4 Design Parameters. Three design parameters are defined: (1) number of uniaxial first-order unit cells N_c that make up a second-order unit cell, (2) length of first-order unit cells L_c , and (3) beam element diameter ϕ (Fig. 4).

Scaffolds have three-dimensional symmetry with an equal number of uniaxial first-order unit cells N_c in x , y , and z directions.

**Fig. 2 Multilevel scaffold design**

Beam elements are generated with circular cross sections. Hierarchical scaffolds consist of two layers of first-order unit cells that make up their outside borders (Fig. 4).

Four nodes at element intersections are indicated with white circles in Fig. 4. Each node is spaced one unit cell length L_c apart on a given axis. Dimensions $L_1 = L_c - \phi$, $L_2 = \phi/\sqrt{2}$, $L_3 = L_1 - L_2$, and $L_4 = \sqrt{2}L_3$ are calculated among elements with width ϕ oriented at 45 deg or 90 deg. In Fig. 4, three shading levels indicate the material volume attributed to scaffold nodes (darkest), straight elements, and diagonal elements (lightest) used in property calculations.

3.5 Property Calculations. Design parameters are used to calculate pore size, volume, porosity, surface area, and elastic modulus properties. Pore size p is the diameter of a sphere inscribed in a unit cell that does not overlap any beam elements [17] such that

$$p = L_c - \phi \quad (1)$$

Scaffold length L_s is its number and length of unit cells, plus the additional length of one element diameter, according to

$$L_s = N_c \cdot L_c + \phi \quad (2)$$

with scaffold volume V_s as

$$V_s = L_s^3 \quad (3)$$

The material volume V_m is found by counting all nodes N_n , the number of straight elements N_b , and the number of diagonal elements N_t ; beam topology types always have zero N_t . Analytical relationships for determining the number of nodes and elements for each topology type are unique and complicated in the case of hierarchical scaffolds. These numbers are, therefore, tracked in the computational environment during scaffold generation.

Material volume is calculated by summing the volume of all nodes, the volume of all straight elements that does not include nodal volume contributions, and the volume of all diagonal elements that does not include nodal or straight element volume contributions such that

$$V_m = N_n \cdot \phi^3 + \frac{\pi\phi^2}{4} \left[N_b \cdot (L_1) + N_t \cdot (L_4) + N_t \cdot \left(\frac{\phi}{3}\right) \right] \quad (4)$$

The $N_t \cdot (\phi/3)$ term approximates the diagonal element volume for the length they extend beyond L_4 before intersecting with straight members. Porosity P is determined by comparing the scaffold material volume to the total nominal volume and subtracting from unity to find

$$P = 1 - \frac{V_m}{V_s} \quad (5)$$

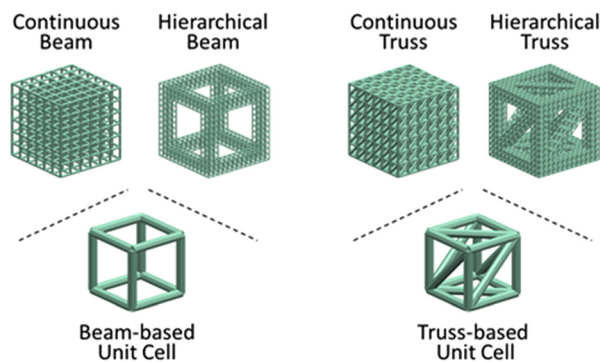


Fig. 3 Scaffold topology types

Surface area depends on the first-order unit cell type, because surfaces of straight elements are partially covered when diagonal elements are present. To simplify mathematical calculations, nodal contributions are assumed negligible, since most nodes exist at beam intersections and have no exposed surfaces. Nodes also have small surface area contributions for scaffolds with high porosities that generally have elements with relatively long lengths and small diameters. Surface area for scaffolds with beam unit cells S_b is

$$S_b = \pi \phi \cdot (N_b \cdot L_1) \quad (6)$$

while surface area for truss unit cells S_t is

$$S_t = \pi \phi \cdot (N_b \cdot L_3 + N_t \cdot L_4) \quad (7)$$

and surface–volume ratio is

$$S/V = \frac{S_b}{V_s} \text{ or } S/V = \frac{S_t}{V_s} \quad (8)$$

The elastic modulus E_s is found by finite element analysis (FEA) of the scaffold's structure by measuring its reaction forces F when a unidirectional displacement δ is applied to all nodes on its top face. Scaffolds are generated as lists of nodes and members using JAVA and imported in ABAQUS for FEA as beam-based wire-frame models. Boundary conditions are used that fix the scaffold in space by placing a pin in one corner and constraining lateral movement at one other point on the bottom face. A displacement constraint is used on all nodes on the bottom face to simulate a flat surface for mechanical testing. A small value for the elastic modulus of the material is used (1 MPa) and reaction forces are found when the scaffold is displaced less than 5% of the scaffold's length to determine the relative elastic modulus.

Each member's linear elastic behavior is approximated with the Euler–Bernoulli beam theory by dividing the member longitudinally into three equal parts [36]. The elastic modulus of the (cubic) structure is then

$$E_s = \frac{F}{L_s \cdot \delta} \quad (9)$$

and converted to a relative elastic modulus E_r of

$$E_r = \frac{E_s}{E_m} \quad (10)$$

where E_m is the base material's elastic modulus.

4 Parametric Study

A study is conducted to demonstrate how design parameters influence properties for the continuous beam topology, followed by all topology types.

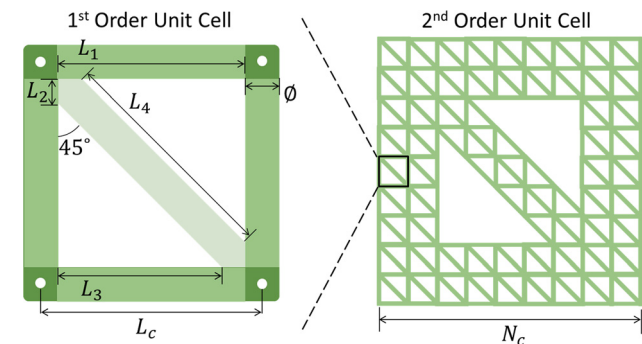


Fig. 4 Planar schematic of hierarchical truss with indicated element diameter ϕ , unit cell length L_c , number of unit cells N_c , and lengths L_1 , L_2 , L_3 , and L_4

4.1 Continuous Beam. Continuous beam topology types are generated using a datum value for the number of unit cells $N_c = 6$, unit cell length $L_c = 1.0$ mm, and element diameter $\phi = 400$ μm . Design parameters are independently perturbed to half and twice the datum value while porosity P , surface–volume ratio S/V , and relative elastic modulus E_c are plotted in Fig. 5.

The number of unit cells does not significantly influence porosity, surface–volume ratio, or relative elastic modulus. These results are expected since scaffold properties should scale with volume when there is no alteration of local structure. The small difference in property values that occurs as the number of unit cells increases is caused by the extra half element diameter added to each side of the scaffold (i.e., when calculating scaffold length in Eq. (2), there is a constant element diameter value included that does not scale with the number of unit cells).

As unit cell length increases, porosity increases and relative elastic modulus decreases since nominal scaffold volume increases faster than the scaffold material volume. Surface–volume ratio initially increases and then decreases. The relation emerges because surface area scales linearly with unit cell length (surface area is proportional to the linear increase in beam element length), while volume increases cubically (since scaffold length in x , y , and z directions scales linearly).

Increases in element diameter decrease porosity and increase relative elastic modulus, while surface–volume ratio initially increases and then decreases. The surface–volume ratio emerges because elements' increasing diameters become proportionally smaller to the decrease in surface area due to elements having greater overlaps that reduce their exposed length. The peak in surface–volume ratio for changes in unit cell length and element diameter suggests the existence of optimal points in the design space. Although porosity and relative elastic modulus are correlated to directional changes in design parameters, they do so non-linearly, which suggest the need for design approaches to aid searches for favorable designs.

4.2 All Topology Types. Each design parameter is swept independently for each topology type from datum values for the number of unit cells $N_c = 10$, unit cell length $L_c = 1.5$ mm, and element diameter $\phi = 1000$ μm . Hierarchical topology types have a minimum number of unit cells, otherwise there is no large central pore and they are identical to continuous topologies with the same parameter values. The large central pore begins forming when the number of unit cells is six or greater for the hierarchical beam topology and seven or greater for hierarchical truss topology. The minimum number of unit cells is dependent on the border size for second-order unit cells, which is chosen as a constant two unit cells (Fig. 4).

Results for porosity, surface–volume ratio, and relative elastic modulus are plotted for each topology type as a function of each swept design parameter in Fig. 6. Truss-based scaffolds are plotted for a smaller range of parameter values because their surface area becomes zero and pores become inaccessible at lower parametric values than occurs for beam-based scaffolds.

As the number of unit cells increases (Fig. 6(a)), the continuous truss topology maintains constant values for each scalable

property, but the hierarchical truss properties do not remain constant. Differences in the hierarchical scaffolds occur because the large central pore removes a larger proportion of scaffold material as more unit cells are added, since there is always a border of two unit cells that make up the outside of the scaffold, as shown in Fig. 4. As the relative size of the large central pore increases, porosity increases, surface–volume ratio decreases, and relative elastic modulus decreases.

As unit cell length and element diameter increases, hierarchical scaffold properties follow qualitatively similar curves to continuous scaffolds. Generally, hierarchical scaffolds have increased porosity, lower surface–volume ratio, and lower relative elastic modulus in comparison to continuous scaffolds. The large central pore causes hierarchical topology types to have a lower number of elements, and therefore less material overall for providing surfaces and bearing load.

Truss-based unit cells tend to have lower porosity, higher surface–volume ratio, and higher relative elastic modulus than beam-based unit cells. These differences occur because the truss-based unit cell contains the same element organization as the beam-based unit cell, plus an additional element on each face.

The difference in continuous beam datum values for Figs. 5 and 6 highlights the sensitivity of univariate searches to initial conditions when exploring the design space. For instance, the highest found surface–volume ratio for continuous beam scaffolds is ~ 3.5 mm^{-1} in Fig. 5 and ~ 2.8 mm^{-1} in Fig. 6. These findings suggest that the need for informed choices in design space sampling to ensure favorable designs are found.

To facilitate design searches, properties such as pore size or porosity may be restricted to relevant values for a particular application, which restricts the design space size. Pore size (Eq. (1)) is identical for all topology types for a given set of design parameters, but not all generated designs have pore sizes suitable for bone tissue engineering (200 μm to 1000 μm). In Sec. 5, designs are generated with a desired pore size held constant.

5 Design Selection

Designs of each topology type are generated with controlled pore size and volume to produce four samples with 80% porosity that are 3D printed. A scaffold with maximized surface–volume ratio is then fabricated as a interbody cage prototype.

5.1 Designs for Experiments. Scaffold samples are constrained to 1.5 cm length and 1000 μm pores. The chosen scaffold dimensions minimize wet-lab and mechanical testing expenses while retaining relevant pore sizes. A constant pore size c is achieved by modifying Eq. (1) to solve for unit cell length $L_c = c + \phi$ as element diameter is adjusted. This modification increases scaffold volume as unit cell length increases, and therefore the number of unit cells requires reduction. When assuming a maximum scaffold length L_m , there is a constraint for number of unit cells $N_c \leq ((L_m - \phi)/L_c)$ to ensure nominal volume constraints are met.

Scaffolds are generated for each topology type by increasing element diameter ϕ from 200 μm to 1400 μm while adjusting L_c

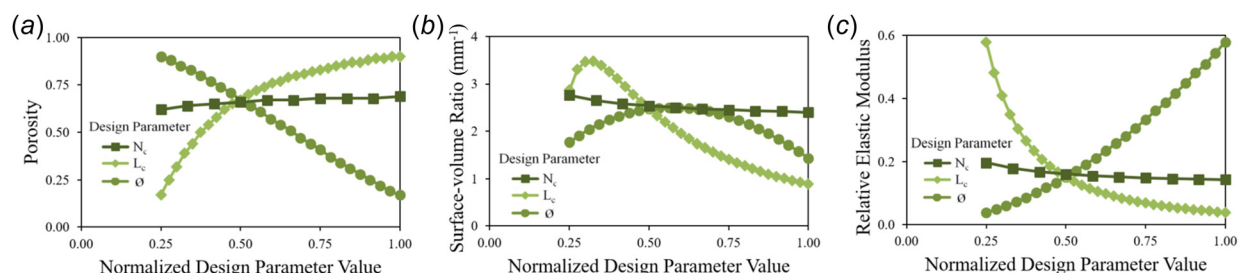


Fig. 5 Continuous beam designs with parameters normalized to $N_c = 12$, $L_c = 2.0$ mm, and $\phi = 800$ μm for (a) porosity, (b) surface–volume ratio, and (c) relative elastic modulus

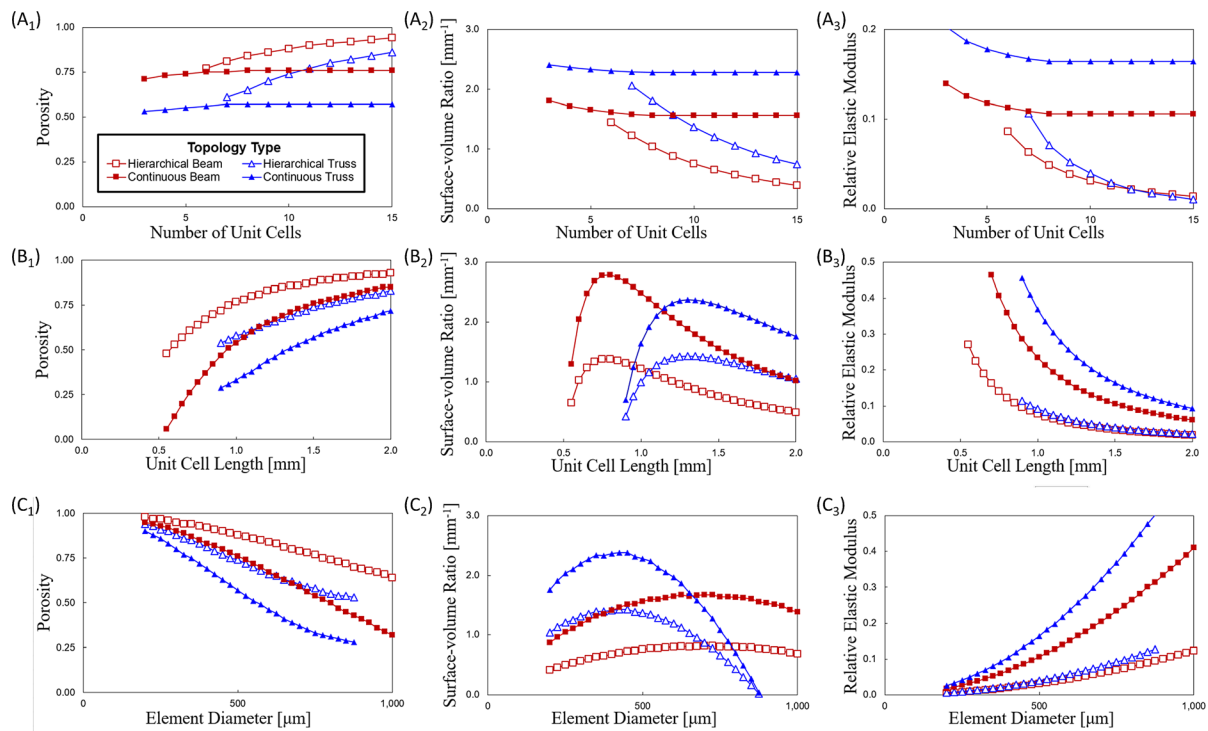


Fig. 6 Designs for each topology type generated by independently sweeping design parameters (a) number of cells N_c , (b) unit cell length L_c , and (c) element diameter ϕ for (A₁, B₁, C₁) porosity, (A₂, B₂, C₂) surface–volume ratio, and (A₃, B₃, C₃) relative elastic modulus

for a constant pore size c of $1000\ \mu\text{m}$ and N_c for a maximum scaffold length L_m of $1.5\ \text{cm}$. Surface–volume ratio and relative elastic modulus are plotted for calculated values in Fig. 7; the data is discontinuous, since N_c is adjusted with integer values.

For a given porosity, continuous and truss-based scaffolds tend to have higher surface–volume ratios, although the continuous beam and hierarchical truss scaffolds have similar surface–volume ratios. There is a maximum achievable surface–volume ratio for each topology type. Continuous and beam-based scaffolds tend to have higher relative elastic moduli, since truss-based scaffolds have a greater proportion of elements not aligned with the compressive loading direction. Scaffolds with 80% porosity, which is suitable for bone tissue engineering, are fabricated [54] and compared in Table 2. Continuous topologies are rescaled to four unit cells to facilitate economic testing.

Table 2 topology types all have unique design parameter values. Scaffolds comparatively have small unit cell lengths with small element diameters, or large unit cell lengths with large element diameters, as demonstrated by the continuous truss and

hierarchical beam, respectively. When selecting designs solely by maximizing surface–volume ratio, the continuous truss topology has the highest surface–volume ratio of $2.7\ \text{mm}^{-1}$; the continuous beam scaffold has the highest relative elastic modulus of 0.091.

Design selection is dependent on multiple factors that are difficult to assess without further information of the scaffold environment experienced once implanted as part of an interbody fusion cage. For instance, too high of a surface area is problematic if it causes scaffold degradation to occur at a faster rate than load-bearing tissues grow to replace the scaffold [44], while an elastic modulus greater than bone's elastic modulus is detrimental if it leads to stress shielding [36]. Additionally, the continuous scaffolds do not offer a large central pore to promote nutrient transport throughout the scaffold [55], which has the potential to limit tissue growth rates.

5.2 Interbody Cage Prototype. Figure 7 designs are plotted in Fig. 8(a) for element diameter, which enables a selection of

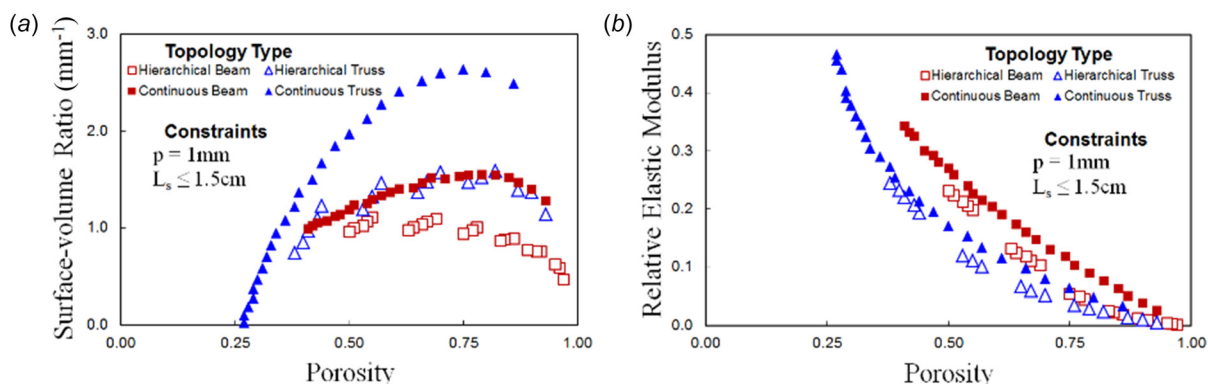
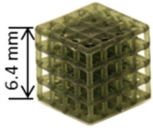
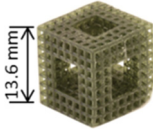
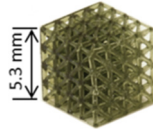
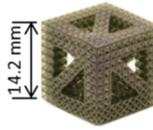


Fig. 7 Designs for each topology type generated by sweeping element diameter ϕ from $200\ \mu\text{m}$ to $1400\ \mu\text{m}$ with pore size $p = 1\ \text{mm}$ and scaffold length $L_s \leq 1.5\ \text{cm}$ for (a) surface–volume ratio and (b) relative elastic modulus

Table 2 Samples with porosity $P \sim 0.8$ and pore size $p=1000 \mu\text{m}$

Topology type	3D printed sample				
		Continuous beam	Hierarchical beam	Continuous truss	Hierarchical truss
Design parameters	Number of axial unit cells (#)	4	8	4	10
	Unit cell length (μm)	1440	1620	1260	1380
	Element diameter (μm)	440	620	260	380
Scaffold properties	Scaffold length (mm)	6.4	13.6	5.3	14.2
	Pore size (μm)	1000	1000	1000	1000
	Porosity	0.79	0.79	0.80	0.80
	Surface-volume ratio (mm^{-1})	1.6	1.0	2.7	1.5
	Relative elastic modulus	0.091	0.049	0.044	0.028

designs in relation to manufacturing features such as the minimum printable element diameter [54]. A hierarchical truss design is selected with a maximized surface–volume ratio and porosity of 0.73, which reflects design features conducive for bone tissue growth. Namely, that the scaffold has a high surface area for initial cell attachment, large pores for nutrient transport, and future material selection can ensure an appropriate elastic modulus. The tailored scaffold sample is 3D printed in a rectangular patterning of six second-order unit cells in Fig. 8(b).

The scaffold sample measures 21.1 mm by 31.1 mm laterally and 13.5 mm in height, with visible triangular pores for both first- and second-order unit cells. These results demonstrate as proof-of-concept the potential to design and fabricate tailored structures for spinal fusion applications via the developed multilevel design approach.

6 Discussion

The developed computational approach supports parametric generation and assessment of tissue scaffolds when considering mechanical and biological factors. 3D printed scaffold samples were fabricated as proof of concepts for experimental testing and use in interbody fusion cages, which presents a foundation for further tissue scaffold design and manufacturing. The computational approach enables rapid design space exploration via assessment of scaffold properties prior to fine-tuning designs using more expensive simulations and experiments.

Simulations informed from existing experimental data are available for assessing scaffold permeability [29,56], mechanics [36], vasculature growth [45], and tissue generation [57–59]. Mechanical simulations that model structures as solids rather than wireframes (Sec. 3.5) could potentially provide higher accuracy. However, inaccuracies are reduced for wireframe evaluations as porosity

increases, since the length to width ratio of beams generally increases with scaffold porosity. Therefore, inaccuracies in design selection are minimized since high scaffold porosities of up to 90% are generally desired. Relative differences in evaluated mechanics between topology types should remain similar among computational methods and may be validated with mechanical testing.

Computational methods that encourage rapid design space exploration are useful when considering the multivariable scaffold design space and its unimodal nonlinear relations. Such computational searches can provide a better design space characterization in comparison to resource expensive scientific experiments or simulations that typically rely on manipulating one variable at a time [3]. When limited to manipulating one variable at a time, the starting point in univariate search can significantly bias design space searches, as demonstrated by the difference in maximum surface–volume ratio when comparing Figs. 5 and 6 continuous beam topologies ($\sim 3.5 \text{ mm}^{-1}$ and $\sim 2.6 \text{ mm}^{-1}$, respectively). Computational search is necessary for finding favorable designs prior to testing and fabrication, where early findings can reduce later costs by isolating highly favorable designs through iterative and broad design space exploration [60].

Once computational methods have determined preferred designs, a suitable printing process and material may be selected. Scaffold prototypes in Table 2 and Fig. 8 were fabricated with an acrylic polymer using a stereolithography process [54]. Stereolithography processes are capable of printing biocompatible structures with polylactic acid-based resins [10]. Alternatively, it is possible to use an indirect fabrication process to mold the scaffold and recreate its form with an appropriate biocompatible material that maintains the features achieved from the 3D printing process [61,62]. A benefit in the indirect approach is the potential to fabricate scaffolds with complex forms enabled by 3D printing using

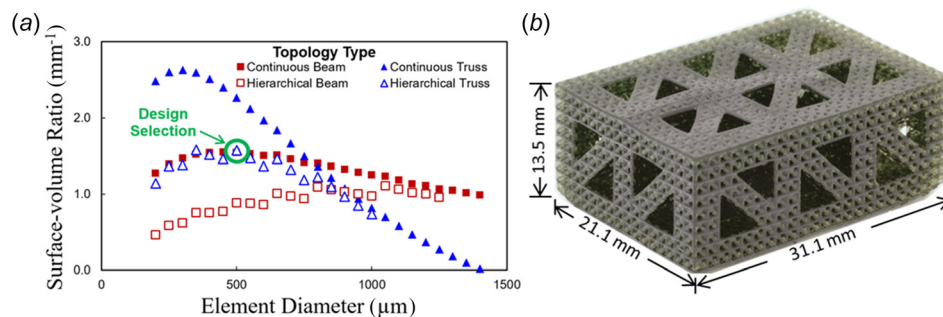


Fig. 8 (a) Data from Fig. 7(a) replotted for element diameter ϕ . A hierarchical truss with number of cells $N_c = 9$, cell length $L_c = 1.5 \text{ mm}$, and element diameter $\phi = 500 \mu\text{m}$ is selected and (b) patterned with dimensions relevant for an interbody cage; note that adjacent second-order unit cells share first-order unit cells when patterned to form a tailored structure.

biomaterials that are traditionally not suitable for 3D printing processes. Alternatively, titanium scaffolds may be constructed using selective laser sintering processes. Titanium scaffolds may benefit from the large central pore in hierarchical structures that would lower global scaffold stiffness and mitigate stress shielding issues from titanium's higher elastic modulus [36].

Imaging processes such as X-ray microtomography are well-suited for assessing the accuracy of printed scaffolds through comparison of a 3D imaging of the fabricated structure with its CAD file. Stereolithography processes have achieved a strong agreement between model and fabrication for designs with features similar to the scaffolds in Table 2 [10]. Fabrication inaccuracies are reducible by altering designs to have larger features or adjusting print processing parameters [63]. For instance, circular element cross sections facilitate smaller printing dimensions when resin cures symmetrically around projected light since a circular shape is naturally formed (for elements aligned with the print direction). A square shape, in comparison, would likely require a larger fabricated area to accurately reproduce.

Once fabricated forms are validated, designs may be assessed with mechanical testing or with tissue culture where imaging is used to determine tissue growth over time. Testing is necessary when design decisions are difficult to evaluate, such as the most appropriate size for the large central pore in hierarchical structures and whether it provides benefits over continuous scaffolds with no central pore [25]. The large central pore's size may be tuned through altering the number of border cells used to generate the hierarchy, in addition to the number of unit cells used to generate a second-order unit cell. Testing would also be required to determine if differences in permeability and tissue growth rate occur due to the different interconnectivities of the beam and truss-based unit cells. The smaller triangular pores of the truss-based unit cell may reduce permeability [56] through increased surface area while promoting faster tissue growth [58].

The developed, systematic design approach is potentially generalizable with steps of design parameterization, generation, and selection based on rational choices, rather than trial-and-error approaches common for tissue engineering [13]. The approach is potentially applicable to further tissue types beyond bone, such as cartilage or cardiac tissue [64], since it focuses on tuning the structure rather than requiring biochemical strategies targeting specific tissues. Further design considerations for fully exploring the design space are constrained pore sizes beyond than the 1 mm considered for Fig. 7, tuned ratios between local porosity to global porosity of hierarchical scaffolds, and the alternation of diagonal element directionality in adjacent truss-based unit cells.

7 Conclusion

Mechanical and biological factors were used to assess parametrically generated tissue scaffolds with multilevel organization. Four topology types were generated by continuously or hierarchically patterning beam or truss-based unit cells. For a given porosity, scaffolds with beam-based unit cells have higher elastic moduli while truss-based scaffolds tend to reach greater surface-volume ratios. Hierarchical designs contain large pores that encourage nutrient transport but reduce surface-volume ratio and elastic modulus. Scaffolds designed with 80% porosity and 1 mm pores were 3D printed as a basis for scientifically comparing each topology type. A hierarchical truss scaffold configured with a maximized surface-volume ratio was fabricated as a to-scale prototype for an interbody fusion cage. The paper demonstrates the linking of fabrication process, structural design, scaffold properties, and design performance as a promising route for developing engineering design methods that aid product development for regenerative medicine.

Acknowledgment

Funding support was provided by ETH Zurich's postdoctoral research fellowship program. An early iteration of this paper was

published at the 2016 ASME International Design Engineering and Technical Conference [54].

References

- [1] Egan, P., Sinko, R., LeDuc, P., and Keten, S., 2015, "The Role of Mechanics in Biological and Synthetic Bio-Inspired Systems," *Nat. Commun.*, **6**, p. 7418.
- [2] Egan, P., Cagan, J., Schunn, C., Chiu, F., Moore, J., and LeDuc, P., 2016, "The D3 Methodology: Bridging Science and Design for Bio-Based Product Development," *ASME J. Mech. Des.*, **138**(8), p. 081101.
- [3] Egan, P., Schunn, C., Cagan, J., and LeDuc, P., 2015, "Improving Human Understanding and Design of Complex Multi-Level Systems With Animation and Parametric Relationship Supports," *Des. Sci.*, **1**(e3), pp. 1–31.
- [4] Fisher, M. B., and Mauck, R. L., 2013, "Tissue Engineering and Regenerative Medicine: Recent Innovations and the Transition to Translation," *Tissue Eng., Part B*, **19**(1), pp. 1–13.
- [5] Liu, Y., Lim, J., and Teoh, S.-H., 2013, "Review: Development of Clinically Relevant Scaffolds for Vascularised Bone Tissue Engineering," *Bioelectron. Adv.*, **31**(5), pp. 688–705.
- [6] Buonasegna, E., Salomo, S., Maier, A. M., and Li-Ying, J., 2014, "Pharmaceutical New Product Development: Why do Clinical Trials Fail?," *R&D Manage.*, **44**(2), pp. 189–202.
- [7] Hollister, S. J., and Murphy, W. L., 2011, "Scaffold Translation: Barriers Between Concept and Clinic," *Tissue Eng., Part B*, **17**(6), pp. 459–474.
- [8] Habib, F. N., Nikzad, M., Masood, S. H., and Saifullah, A. B. M., 2016, "Design and Development of Scaffolds for Tissue Engineering Using Three-Dimensional Printing for Bio-Based Applications," *3D Print. Addit. Manuf.*, **3**(2), pp. 119–127.
- [9] Derby, B., 2012, "Printing and Prototyping of Tissues and Scaffolds," *Science*, **338**(6109), pp. 921–926.
- [10] Melchels, F. P., Bertoldi, K., Gabbriellini, R., Velders, A. H., Feijen, J., and Grijpma, D. W., 2010, "Mathematically Defined Tissue Engineering Scaffold Architectures Prepared by Stereolithography," *Biomaterials*, **31**(27), pp. 6909–6916.
- [11] Stanković, T., Mueller, J., Egan, P., and Shea, K., 2015, "A Generalized Optimality Criteria Method for Optimization of Additively Manufactured Multiscale Lattice Structures," *ASME J. Mech. Des.*, **137**(11), p. 111705.
- [12] Byrne, D. P., Lacroix, D., Planell, J. A., Kelly, D. J., and Prendergast, P. J., 2007, "Simulation of Tissue Differentiation in a Scaffold as a Function of Porosity, Young's Modulus and Dissolution Rate: Application of Mechanobiological Models in Tissue Engineering," *Biomaterials*, **28**(36), pp. 5544–5554.
- [13] Boccaccio, A., Uva, A. E., Fiorentino, M., Lamberti, L., and Monno, G., 2016, "A Mechanobiology-Based Algorithm to Optimize the Microstructure Geometry of Bone Tissue Scaffolds," *Int. J. Biol. Sci.*, **12**(1), p. 1.
- [14] Geris, L., Guyot, Y., Schrooten, J., and Papantonou, I., 2016, "In Silico Regenerative Medicine: How Computational Tools Allow Regulatory and Financial Challenges to be Addressed in a Volatile Market," *Interface Focus*, **6**(2), p. 20150105.
- [15] Giannitelli, S., Accoto, D., Trombetta, M., and Rainer, A., 2014, "Current Trends in the Design of Scaffolds for Computer-Aided Tissue Engineering," *Acta Biomater.*, **10**(2), pp. 580–594.
- [16] Sanz-Herrera, J., García-Aznar, J., and Doblaré, M., 2009, "On Scaffold Designing for Bone Regeneration: A Computational Multiscale Approach," *Acta Biomater.*, **5**(1), pp. 219–229.
- [17] Naing, M., Chua, C., Leong, K., and Wang, Y., 2005, "Fabrication of Customised Scaffolds Using Computer-Aided Design and Rapid Prototyping Techniques," *Rapid Prototyping J.*, **11**(4), pp. 249–259.
- [18] Bose, S., Roy, M., and Bandyopadhyay, A., 2012, "Recent Advances in Bone Tissue Engineering Scaffolds," *Trends Biotechnol.*, **30**(10), pp. 546–554.
- [19] Guldberg, R., Caldwell, N., Guo, X., Goulet, R., Hollister, S., and Goldstein, S., 1997, "Mechanical Stimulation of Tissue Repair in the Hydraulic Bone Chamber," *J. Bone Mineral Res.*, **12**(8), pp. 1295–1302.
- [20] Baas, E., Kuiper, J. H., Yang, Y., Wood, M. A., and El Haj, A. J., 2010, "In Vitro Bone Growth Responds to Local Mechanical Strain in Three-Dimensional Polymer Scaffolds," *J. Biomech.*, **43**(4), pp. 733–739.
- [21] Rumpel, M., Woesz, A., Dunlop, J. W., van Dongen, J. T., and Fratzl, P., 2008, "The Effect of Geometry on Three-Dimensional Tissue Growth," *J. R. Soc. Interface*, **5**(27), pp. 1173–1180.
- [22] Polikeit, A., Ferguson, S. J., Nolte, L. P., and Orr, T. E., 2003, "Factors Influencing Stresses in the Lumbar Spine After the Insertion of Intervertebral Cages: Finite Element Analysis," *Eur. Spine J.*, **12**(4), pp. 413–420.
- [23] Abbah, S. A., Lam, C. X., Huttmacher, D. W., Goh, J. C., and Wong, H.-K., 2009, "Biological Performance of a Polycaprolactone-Based Scaffold Used as Fusion Cage Device in a Large Animal Model of Spinal Reconstructive Surgery," *Biomaterials*, **30**(28), pp. 5086–5093.
- [24] Bashkuev, M., Checa, S., Postigo, S., Duda, G., and Schmidt, H., 2015, "Computational Analyses of Different Intervertebral Cages for Lumbar Spinal Fusion," *J. Biomech.*, **48**(12), pp. 3274–3282.
- [25] Yamada, K., Ito, M., Akazawa, T., Murata, M., Yamamoto, T., and Iwasaki, N., 2015, "A Preclinical Large Animal Study on a Novel Intervertebral Fusion Cage Covered With High Porosity Titanium Sheets With a Triple Pore Structure Used for Spinal Fusion," *Eur. Spine J.*, **24**(11), pp. 2530–2537.
- [26] Zhong, Z.-C., Wei, S.-H., Wang, J.-P., Feng, C.-K., Chen, C.-S., and Yu, C.-H., 2006, "Finite Element Analysis of the Lumbar Spine With a New Cage Using a Topology Optimization Method," *Med. Eng. Phys.*, **28**(1), pp. 90–98.
- [27] Otto, K. N., Hölttä-Otto, K., Simpson, T. W., Krause, D., Ripperda, S., and Moon, S. K., 2016, "Global Views on Modular Design Research: Linking Alternative Methods to Support Modular Product Family Concept Development," *ASME J. Mech. Des.*, **138**(7), p. 071101.

- [28] Hollister, S. J., Flanagan, C. L., Zopf, D. A., Morrison, R. J., Nasser, H., Patel, J. J., Ebramzadeh, E., Sangiorgio, S. N., Wheeler, M. B., and Green, G. E., 2015, "Design Control for Clinical Translation of 3D Printed Modular Scaffolds," *Ann. Biomed. Eng.*, **43**(3), pp. 774–786.
- [29] Olivares, A. L., Marsal, È., Planell, J. A., and Lacroix, D., 2009, "Finite Element Study of Scaffold Architecture Design and Culture Conditions for Tissue Engineering," *Biomaterials*, **30**(30), pp. 6142–6149.
- [30] Iura, A., McNerny, E. G., Zhang, Y., Kamiya, N., Tantillo, M., Lynch, M., Kohn, D. H., and Mishina, Y., 2015, "Mechanical Loading Synergistically Increases Trabecular Bone Volume and Improves Mechanical Properties in the Mouse When BMP Signaling is Specifically Ablated in Osteoblasts," *PLoS One*, **10**(10), p. e0141345.
- [31] Woodard, J. R., Hilladore, A. J., Lan, S. K., Park, C., Morgan, A. W., Eurell, J. A. C., Clark, S. G., Wheeler, M. B., Jamison, R. D., and Johnson, A. J. W., 2007, "The Mechanical Properties and Osteoconductivity of Hydroxyapatite Bone Scaffolds With Multi-Scale Porosity," *Biomaterials*, **28**(1), pp. 45–54.
- [32] Laschke, M., Strohe, A., Scheuer, C., Eglon, D., Verrier, S., Alini, M., Pohlemann, T., and Menger, M., 2009, "In Vivo Biocompatibility and Vascularization of Biodegradable Porous Polyurethane Scaffolds for Tissue Engineering," *Acta Biomater.*, **5**(6), pp. 1991–2001.
- [33] Olson, G. B., 1997, "Computational Design of Hierarchically Structured Materials," *Science*, **277**(5330), pp. 1237–1242.
- [34] Loh, Q. L., and Choong, C., 2013, "Three-Dimensional Scaffolds for Tissue Engineering Applications: Role of Porosity and Pore Size," *Tissue Eng., Part B*, **19**(6), pp. 485–502.
- [35] Sicchieri, L. G., Crippa, G. E., de Oliveira, P. T., Beloti, M. M., and Rosa, A. L., 2012, "Pore Size Regulates Cell and Tissue Interactions With PLGA–CaP Scaffolds Used for Bone Engineering," *J. Tissue Eng. Regen. Med.*, **6**(2), pp. 155–162.
- [36] Wieding, J., Wolf, A., and Bader, R., 2014, "Numerical Optimization of Open-Porous Bone Scaffold Structures to Match the Elastic Properties of Human Cortical Bone," *J. Mech. Behav. Biomed. Mater.*, **37**, pp. 56–68.
- [37] Minardi, S., Corradetti, B., Taraballi, F., Sandri, M., Van Eps, J., Cabrera, F., Weiner, B. K., Tampieri, A., and Tasciotti, E., 2015, "Evaluation of the Osteoinductive Potential of a Bio-Inspired Scaffold Mimicking the Osteogenic Niche for Bone Augmentation," *Biomaterials*, **62**, pp. 128–137.
- [38] Fielding, G. A., Bandyopadhyay, A., and Bose, S., 2012, "Effects of Silica and Zinc Oxide Doping on Mechanical and Biological Properties of 3D Printed Tricalcium Phosphate Tissue Engineering Scaffolds," *Dent. Mater.*, **28**(2), pp. 113–122.
- [39] Meza, L. R., Zelhofer, A. J., Clarke, N., Mateos, A. J., Kochmann, D. M., and Greer, J. R., 2015, "Resilient 3D Hierarchical Architected Metamaterials," *Proc. Natl. Acad. Sci.*, **112**(37), pp. 11502–11507.
- [40] Zheng, X., Lee, H., Weisgraber, T. H., Shusteff, M., DeOtte, J., Duoss, E. B., Kuntz, J. D., Biener, M. M., Ge, Q., and Jackson, J. A., 2014, "Ultralight, Ultra-stiff Mechanical Metamaterials," *Science*, **344**(6190), pp. 1373–1377.
- [41] O'Brien, F. J., 2011, "Biomaterials & Scaffolds for Tissue Engineering," *Mater. Today*, **14**(3), pp. 88–95.
- [42] McKeen, L. W., 2014, *Plastics Used in Medical Devices*, William Andrew Publishing, Oxford, UK, Chap. 3.
- [43] Wu, L., and Ding, J., 2004, "In Vitro Degradation of Three-Dimensional Porous Poly (D, L-Lactide-co-Glycolide) Scaffolds for Tissue Engineering," *Biomaterials*, **25**(27), pp. 5821–5830.
- [44] Chen, Y., Zhou, S., and Li, Q., 2011, "Microstructure Design of Biodegradable Scaffold and Its Effect on Tissue Regeneration," *Biomaterials*, **32**(22), pp. 5003–5014.
- [45] Mehdizadeh, H., Bayrak, E. S., Lu, C., Somo, S. I., Akar, B., Brey, E. M., and Cinar, A., 2015, "Agent-Based Modeling of Porous Scaffold Degradation and Vascularization: Optimal Scaffold Design Based on Architecture and Degradation Dynamics," *Acta Biomater.*, **27**, pp. 167–178.
- [46] Cheah, C., Chua, C., Leong, K., and Chua, S., 2003, "Development of a Tissue Engineering Scaffold Structure Library for Rapid Prototyping—Part 1: Investigation and Classification," *Int. J. Adv. Manuf. Technol.*, **21**(4), pp. 291–301.
- [47] Cheah, C., Chua, C., Leong, K., and Chua, S., 2003, "Development of a Tissue Engineering Scaffold Structure Library for Rapid Prototyping—Part 2: Parametric Library and Assembly Program," *Int. J. Adv. Manuf. Technol.*, **21**(4), pp. 302–312.
- [48] Fu, K., Moreno, D., Yang, M., and Wood, K., 2014, "Bio-Inspired Design: An Overview Investigating Open Questions From the Broader Field of Design-by-Analogy," *ASME J. Mech. Des.*, **136**(11), p. 111102.
- [49] Cheong, H., and Shu, L., 2014, "Retrieving Causally Related Functions From Natural-Language Text for Biomimetic Design," *ASME J. Mech. Des.*, **136**(8), p. 081008.
- [50] Cohen, Y. H., Reich, Y., and Greenberg, S., 2014, "Biomimetics: Structure–Function Patterns Approach," *ASME J. Mech. Des.*, **136**(11), p. 111108.
- [51] Nagel, J. K., Nagel, R. L., Stone, R. B., and McAdams, D. A., 2010, "Function-Based, Biologically Inspired Concept Generation," *Artif. Intell. Eng. Des. Anal. Manuf.*, **24**(04), pp. 521–535.
- [52] Ashby, M., 2006, "The Properties of Foams and Lattices," *Philos. Trans. R. Soc., A*, **364**(1838), pp. 15–30.
- [53] Vetsch, J. R., Müller, R., and Hofmann, S., 2013, "The Evolution of Simulation Techniques for Dynamic Bone Tissue Engineering in Bioreactors," *J. Tissue Eng. Regen. Med.*, **9**(8), pp. 903–917.
- [54] Egan, P., Ferguson, S., and Shea, K., 2016, "Design and 3D Printing of Hierarchical Tissue Engineering Scaffolds Based on Mechanics and Biology Perspectives," *ASME Paper No. DETC2016-59554*.
- [55] Jonitz-Heincke, A., Wieding, J., Schulze, C., Hansmann, D., and Bader, R., 2013, "Comparative Analysis of the Oxygen Supply and Viability of Human Osteoblasts in Three-Dimensional Titanium Scaffolds Produced by Laser-Beam or Electron-Beam Melting," *Materials*, **6**(11), pp. 5398–5409.
- [56] Truscetto, S., Kerckhofs, G., Van Bael, S., Pyka, G., Schrooten, J., and Van Oosterwyck, H., 2012, "Prediction of Permeability of Regular Scaffolds for Skeletal Tissue Engineering: A Combined Computational and Experimental Study," *Acta Biomater.*, **8**(4), pp. 1648–1658.
- [57] Khayyeri, H., Checa, S., Tägil, M., and Prendergast, P. J., 2009, "Corroboration of Mechanobiological Simulations of Tissue Differentiation in an In Vivo Bone Chamber Using a Lattice-Modeling Approach," *J. Orthop. Res.*, **27**(12), pp. 1659–1666.
- [58] Guyot, Y., Papantoniou, I., Chai, Y. C., Van Bael, S., Schrooten, J., and Geris, L., 2014, "A Computational Model for Cell/ECM Growth on 3D Surfaces Using the Level Set Method: A Bone Tissue Engineering Case Study," *Bio-mech. Model. Mechanobiol.*, **13**(6), pp. 1361–1371.
- [59] Thorne, B. C., Bailey, A. M., and Peirce, S. M., 2007, "Combining Experiments With Multi-Cell Agent-Based Modeling to Study Biological Tissue Patterning," *Briefings Bioinf.*, **8**(4), pp. 245–257.
- [60] Boehm, B. W., 1988, "A Spiral Model of Software Development and Enhancement," *Computer*, **21**(5), pp. 61–72.
- [61] Kang, H.-W., and Cho, D.-W., 2012, "Development of an Indirect Stereolithography Technology for Scaffold Fabrication With a Wide Range of Biomaterial Selectivity," *Tissue Eng., Part C*, **18**(9), pp. 719–729.
- [62] Li, X., Li, D., Lu, B., and Wang, C., 2008, "Fabrication of Bioceramic Scaffolds With Pre-Designed Internal Architecture by Gel Casting and Indirect Stereolithography Techniques," *J. Porous Mater.*, **15**(6), pp. 667–671.
- [63] Mueller, J., Shea, K., and Daraio, C., 2015, "Mechanical Properties of Parts Fabricated With Inkjet 3D Printing Through Efficient Experimental Design," *Mater. Des.*, **86**, pp. 902–912.
- [64] Walser, J., Stok, K. S., Caversaccio, M. D., and Ferguson, S. J., 2016, "Direct Electrospinning of 3D Auricle-Shaped Scaffolds for Tissue Engineering Applications," *Biofabrication*, **8**(2), p. 025007.